J Mater Sci: Mater Electron (2026) 37:406

Electrodes of $Ti_3C_2T_x$ MXene-modified cotton fabrics for wearable triboelectric nanogenerators

Iuri Custódio Montes Cândido[1], Murilo Henrique Moreira Facure[2], Daniel Souza Correa[3], Emanuel Carrilho[4], Joaquim Júnior Isídio de Lima[1], Hernane da Silva Barud[5], and Helinando Pequeno de Oliveira[1,*]

[1] *Instituto de Pesquisa em Ciência dos Materiais, Universidade Federal do Vale do São Francisco, Juazeiro, BA 48902-300, Brazil*
[2] *Departamento de Engenharia de Materiais, Escola de Engenharia de São Carlos (EESC), Universidade de São Paulo (USP), 13563-120, São Carlos, SP, Brazil*
[3] *Laboratório Nacional de Nanotecnologia Aplicada ao Agronegócio (LNNA), Embrapa Instrumentação, São Carlos, SP 13560-970, Brazil*
[4] *Instituto de Química de São Carlos, Universidade de São Paulo, São Carlos, SP 13566-590, Brazil*
[5] *Laboratório de Biopolímeros e Biomateriais (BioPolMat), University of Araraquara, Araraquara, SP 14801-320, Brazil*

Received: 24 December 2025
Accepted: 5 February 2026

ABSTRACT

Metal-free devices are critical components for incorporation into wearables due to comfort and flexibility requirements, as well as the drawbacks of oxidation and skin contact, making modified textiles with conductive fillers promising electrode materials. Herein, $Ti_3C_2T_x$ MXene is incorporated into a cotton textile, which uses a single electrode triboelectric nanogenerator (TENG) with the skin and an Ecoflex layer as tribopairs. This combination results in a device with an open-circuit voltage of 220.5 V, yielding a maximum power density of 42 μW/cm^2, opening the door to promising applications for devices activated by simple finger touch. As a proof of concept, a two-level system for communication with hospital patients is provided by combining two TENGs disposed as tactile sensors in the input of a microcontroller with an output in a speaker, making it possible to communicate with minimal finger movement, with the skin considered as a tribopositive layer in the assembled TENG.

1 Introduction

The rapid growth of wearables and portable electronics technology reinforces the demand for highly efficient power sources [1–3]. However, conventional batteries used in these devices often suffer from critical limitations, including short lifespans, rigid structures, and environmental issues [4]. Developing self-powered devices (battery-free systems) involves devising energy-harvesting methods to convert mechanical energy into electrical energy. In particular, triboelectric nanogenerators (TENGs), invented by Wang and collaborators [5], enable energy harvesting via contact electrification and electrostatic induction. These devices are considered promising components for the next-generation wearable

Address correspondence to E-mail: helinando.oliveira@univasf.edu.br

https://doi.org/10.1007/s10854-026-16790-3
Published online: 21 February 2026

electronics, biosensors, and self-powered healthcare devices [6], with outstanding properties including a lightweight design, low production costs, and operation driven by multiple mechanical input sources [4].

The standard contact-separation TENG mode is schematically illustrated in Fig. S1a. In this configuration, two induction electrodes are placed in contact with the friction layers, in a typical association of capacitors with three dielectric layers in series: a tribopositive and a tribonegative layer with thickness d_1 and d_2 with dielectric constants k_1 and k_2, respectively, and a central gap represented by an air capacitor with thickness $x(t)$ that varies during successive contact and separation cycles. As a consequence, Maxwell's equation for the stationary condition (Eqs. S1 to S4) must consider the modification in the displacement vector by an extra term (P_S) that introduces the effects of the charges that appear in the medium due to the triboelectrification (see Eq. S5). As a result, the expanded Maxwell's equations applied to moving charges are presented in Eqs. S6 to S9. Based on these conditions, the expected values for the open circuit voltage and short-circuit current are given by Eqs. S10 and S11, respectively [7].

Despite promising advantages, a typical limitation for standard TENG-related devices is the lack of wearability of metallic electrodes due to their rigidity and associated issues of comfort and reliability in humid conditions [8]. The configuration of a single electrode (schematically illustrated in Fig. S1b) reduces the number of electrodes in the overall device. It can be explored in a configuration in which the skin is considered a tribopositive layer (the scheme is shown in Fig. S1c), with the corresponding equivalent circuit shown in Fig. S1d, where R_B and C_B represent the resistance and capacitance of the body, respectively.

The development of metal-free conductive electrodes has relied on the incorporation of conductive fillers, in which electrical conductivity is a key parameter alongside adaptability and biocompatibility. In this context, alternative materials have emerged as promising candidates for TENG production, such as carbon derivatives (carbon fiber paper [9] and carbon black [10]), conducting polymers [11, 12], laser-induced graphene (LIG) [13], and graphene-based materials [14], which can act as efficient current collectors while preserving mechanical compliance [8]. In this context, efforts have focused on using natural and bio-based substrates combined with conductive fillers in TENG architectures to improve adaptability and biocompatibility [15].

Recently, significant attention has been given to textiles, versatile supports for wearable triboelectric devices, owing to their intrinsic flexibility, breathability, and user comfort [12]. Unlike rigid substrates, fabrics can conform intimately to the human body, ensuring efficient contact with skin while maintaining long-term wearability. This unique combination of structural adaptability and mechanical resilience makes textile-based TENGs attractive for harvesting biomechanical energy from daily activities. Moreover, their seamless integration into garments and accessories allows for continuous electricity generation without interfering with user mobility and comfort, positioning textile-supported TENGs as an ideal platform for developing self-powered wearable systems [16].

Cotton, in particular, is attractive due to its softness, porosity, breathability, and mechanical robustness [17], as well as its hierarchical fibrous network, which offers comfort, flexibility, and a high surface area [18] due to the high density of available sites for charge accumulation. Under functionalization with conductive nanomaterials, cotton fabrics can serve as mechanically robust supports and active current collectors, broadening their role beyond passive substrates [17]. In addition, its widespread availability, comfort, and washability provide an ideal template for fabricating skin-interfacing devices [19].

MXenes, a class of two-dimensional transition metal carbides and nitrides, have recently emerged as promising conductive fillers for next-generation energy devices [20]. Among them, $Ti_3C_2T_x$ MXene combines high electrical conductivity, mechanical flexibility, tunable surface terminations, and strong electronegativity, enabling efficient charge transfer when incorporated into triboelectric systems [21–24]. $Ti_3C_2T_x$ MXene-coated cotton fabrics can form interconnected conductive networks that enhance electron transport without compromising textile flexibility [20]. This approach has significantly boosted TENG performance, facilitating applications in physiological monitoring and wearable sensors [24].

Herein, we report the fabrication of a textile-based TENG in which $Ti_3C_2T_x$ MXene-modified cotton serves as a metal-free electrode. In the assembled system, human skin operates as the tribopositive material and Ecoflex 00–30 as the tribonegative counterpart. This configuration explores the skin-device interface to harvest biomechanical energy, while $Ti_3C_2T_x$

MXene-functionalized cotton provides efficient electron-transport pathways and mechanical resilience. The proposed architecture is systematically evaluated regarding output voltage, current, power density, and stability under repeated cycles, highlighting its potential as a low-cost, sustainable, and wearable energy-harvesting platform. The high sensitivity to finger touch was explored in a two-level communication system in which a single touch suffices to convey information to an electronic system.

2 Materials and methods

2.1 Preparation of $Ti_3C_2T_x$ MXene

The $Ti_3C_2T_x$ MXene synthesis was adapted from a previously reported work [25]. Briefly, 12 mL of HCl and 2.4 mL of HF were added to 5.6 mL of water in a poly(tetrafluoroethylene) (PTFE) container. Then, 1.0 g of the Ti_3AlC_2 MAX phase was slowly added to the solution. The Al etching was conducted for 24 h at 35 °C. The multilayer MXene was obtained by centrifuging the mixture (3500 rpm for 5 min) repeatedly until the pH of the supernatant exceeded 6. The delamination was performed by dispersing the obtained slurry in 50 mL of LiCl solution (0.5 mol/L), stirring for 20 h. Centrifugation steps (3500 rpm for 5 min) were performed to remove the LiCl and collect the delaminated $Ti_3C_2T_x$ when the supernatant turned dark.

2.2 Pre-treatment of cotton fabric

Cotton discs (0.5 mm thick and 20 mm in diameter) were previously treated and cleaned by immersing them in 1 M NaOH (Dinâmica, Brazil) and 0.2 M Na_2CO_3 (Química Moderna, Brazil) aqueous solutions for 2 h. Then, the discs were washed with Milli-Q water to remove residues and impurities. Subsequently, the samples were immersed in alcohol 70% (Química Moderna, Brazil) for 10 min and dried in an oven at 60 °C for 10 min to remove the solvent. The overall process was repeated three times.

2.3 Impregnation of cotton fabric with $Ti_3C_2T_x$ MXene (CMX)

Cotton discs were immersed in 5 mL of a $Ti_3C_2T_x$ MXene stock dispersion (1.8 mg/mL) to uniformly impregnate the fibrous network via bath sonication (40 kHz, 100 W) for 15 min. Then, the discs were rinsed with deionized water to remove unbound nanosheets and dried in an oven at 60 °C for 5 min. This process was repeated 10 times until a uniform, continuous MXene coating was obtained, ensuring complete adsorption and stable anchoring of the nanosheets to the textile. The resulting MXene-functionalized cotton was applied as a conductive electrode layer of the TENG. The corresponding process is schematically presented in Fig. 1a.

2.4 Production of the CMX-TENG

The fabrication process for the CMX-TENG is schematically illustrated in Fig. 1 (a-c). The device comprises two primary components: a triboelectric friction layer and an electrode layer. The friction layer was prepared using silicone rubber (Ecoflex 00–30, Smooth-On, USA). Precursor A (5 g) and precursor B (5 g) were thoroughly mixed and mechanically stirred for 10 min to ensure complete homogenization. A 30 mm segment of 400-grit sandpaper was affixed to an acrylic substrate with adhesive tape to introduce controlled surface roughness, serving as a mold. The polymer mixture was cast onto the mold and cured at ambient temperature for 24 h (Fig. 1b), yielding elastomeric films with a well-defined microtextured surface.

Finally, as depicted in Fig. 1c, the $Ti_3C_2T_x$ MXene-modified cotton electrode was sandwiched between two silicone rubber films acting as frictional counterparts. A copper wire was attached to the textile electrode as an external terminal for charge transfer and electrical measurements.

2.5 Characterization techniques

Absorption spectra in the UV–Vis region were obtained using an aqueous dispersion of the MXene and quartz cuvettes in a Shimadzu UV-1900 spectrophotometer. The FTIR analysis was carried out in a Shimadzu IRPrestige-21 Fourier transform infrared spectrometer via KBr method. The TENG output voltage was measured with a digital oscilloscope (MSO1104Z, Rigol), with the input channel connected to a 100 MΩ LF-250S probe (Minipa). The oscilloscope's input was connected to a circuit with an LMC6001 current amplifier for measuring the short-circuit current. [26] The variation in the force applied to the TENGs was performed in a Crown DBC Digital

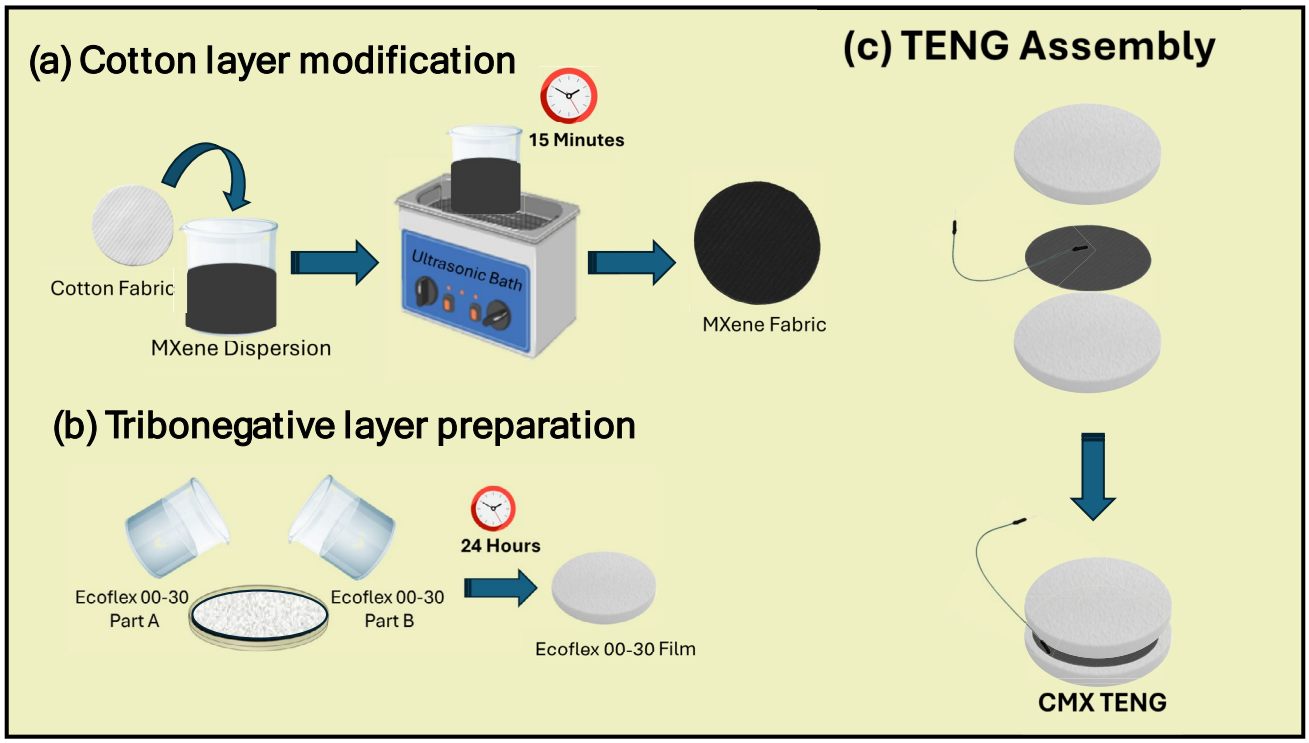

Fig. 1 Schematic representation of **a** the overall process of impregnation of cotton with $Ti_3C_2T_x$ MXene, **b** preparation of the tribonegative layer, and **c** the assembled device

Dynamometer—Oswaldo Filizola (Berman Load Cells—100 kg). The electrical response of the modified cotton textile was evaluated in an Autolab PGSTAT 302N potentiostat/galvanostat (Metrohm) with the material disposed between two parallel plates. A scanning electron microscope (Vega 3XM Tescan) was used to obtain images, with an EDX system that provided overlaid elemental maps for identification.

3 Results and discussion

The structure of the synthesized $Ti_3C_2T_x$ MXene is shown in Fig. 2a, where a typical MXene morphology with layer delamination is evident. The impregnation of textile with $Ti_3C_2T_x$ MXene results in a color change in the coated cotton (Fig. 2b), confirming the successful impregnation of the filler. The SEM image for $Ti_3C_2T_x$ MXene-impregnated cotton fibers in Fig. 2c confirms the disposition of the $Ti_3C_2T_x$ MXene on the cotton fibers, with platelet aggregates observed. EDX overlaid images, shown in Fig. 2d indicate that these are composed of a homogeneous dispersion of Ti elements, which is observed over coated fibers, as identified by red dots. The overlaid image of the $Ti_3C_2T_x$ MXene powder and the corresponding elements map are shown in Figs. S2a and S2b, respectively.

To evaluate the properties of the filler and the impregnated material in cotton textiles, the structural and electronic characterizations of the $Ti_3C_2T_x$ MXene were performed using UV–Vis absorbance, FTIR, and current–voltage curve. The UV–Vis spectrum of an aqueous dispersion of the MXene is shown in Fig. 3a. The MXene spectrum shows a doublet peak at 264 nm and 322 nm that has been attributed to the functionalization of $Ti_3C_2T_x$ MXene by different surface groups (-F, -OH, and -O) [27, 28] and a broad peak in the near infrared region (~ 775 nm) assigned to the surface plasmon vibration in the $Ti_3C_2T_x$ MXene [29, 30]. Regarding the electrical properties of the textile impregnated with $Ti_3C_2T_x$, the ohmic current–voltage curve presented in Fig. 3b shows that a reasonable level of electrical conductivity is observed in the transverse (bulky) direction of the modified textile. A corresponding resistance of 840.3 Ω was obtained with a linear response.

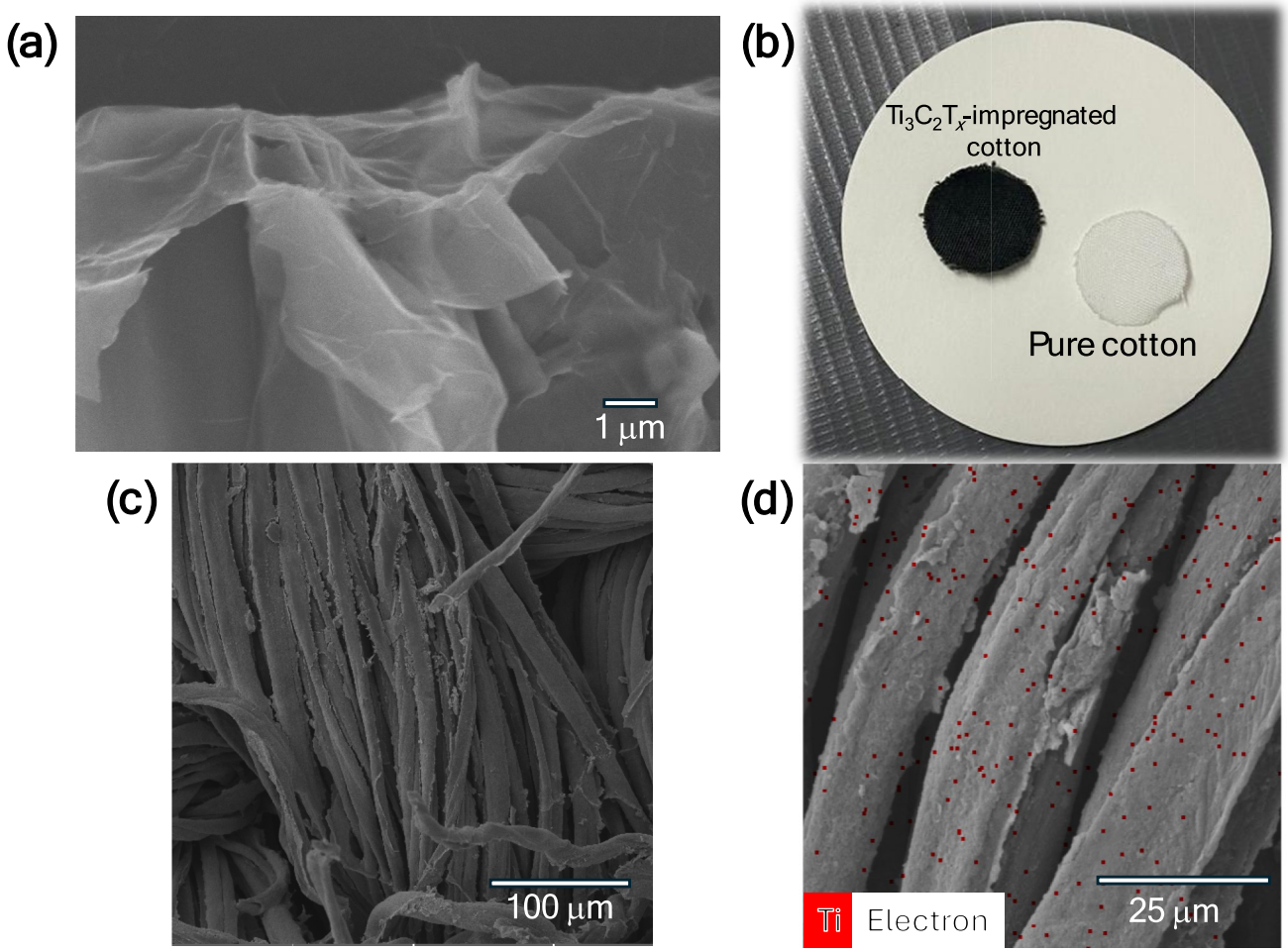

Fig. 2 **a** SEM image of $Ti_3C_2T_x$ MXene with magnification level of 10 kx, **b** photo of pristine cotton textile and impregnated cotton textile with $Ti_3C_2T_x$ MXene, **c** SEM image of cotton textile impregnated with $Ti_3C_2T_x$ MXene with magnification level of 598x, and **d** overlaid EDX image on SEM image of cotton textile impregnated with $Ti_3C_2T_x$ MXene, indicating the presence of Ti element as red dots

As reported by Parker et al. [31], two specific regions are present in the FTIR: in the 4000–1400 cm^{-1} range for confined water into the structure (region I) and in the 1400–400 cm^{-1} range (region II), in which the fingerprint of the structure is observed. From the FTIR spectrum shown in Fig. 3c, it is possible to identify peaks in region I corresponding to -OH bending vibration at 1632 cm^{-1} and -OH stretching vibration at 3440 cm^{-1}, suggesting the absorption of water within the structure [32]. In addition, characteristic peaks from the MXene structure are observed at 1097 cm^{-1}, attributed to the stretching vibration of C-F group [33] and at 645 cm^{-1}, assigned to the Ti–O stretching vibration [31, 34, 35].

X-ray diffraction (XRD) analysis was previously reported by the authors in Ref. [36] confirming the successful synthesis of $Ti_3C_2T_x$ MXene. The comparison between the diffraction patterns of the Ti_3AlC_2 MAX phase and the corresponding $Ti_3C_2T_x$ film confirmed that the Ti_3AlC_2 sample exhibits the full set of characteristic crystallographic peaks. In contrast, the MXene displays only the (00 l) peaks, indicating effective etching and delamination of the MAX phase, with a higher interlayer spacing in the MXene due to the shift in the (002) peak.

The electrical response of the TENG at different forces and frequencies is presented in Fig. 4. Results in Figs. 4a, 4b, and 4c correspond to the open-circuit voltage at 1 Hz (black), 3 Hz (red), and 5 Hz (blue),

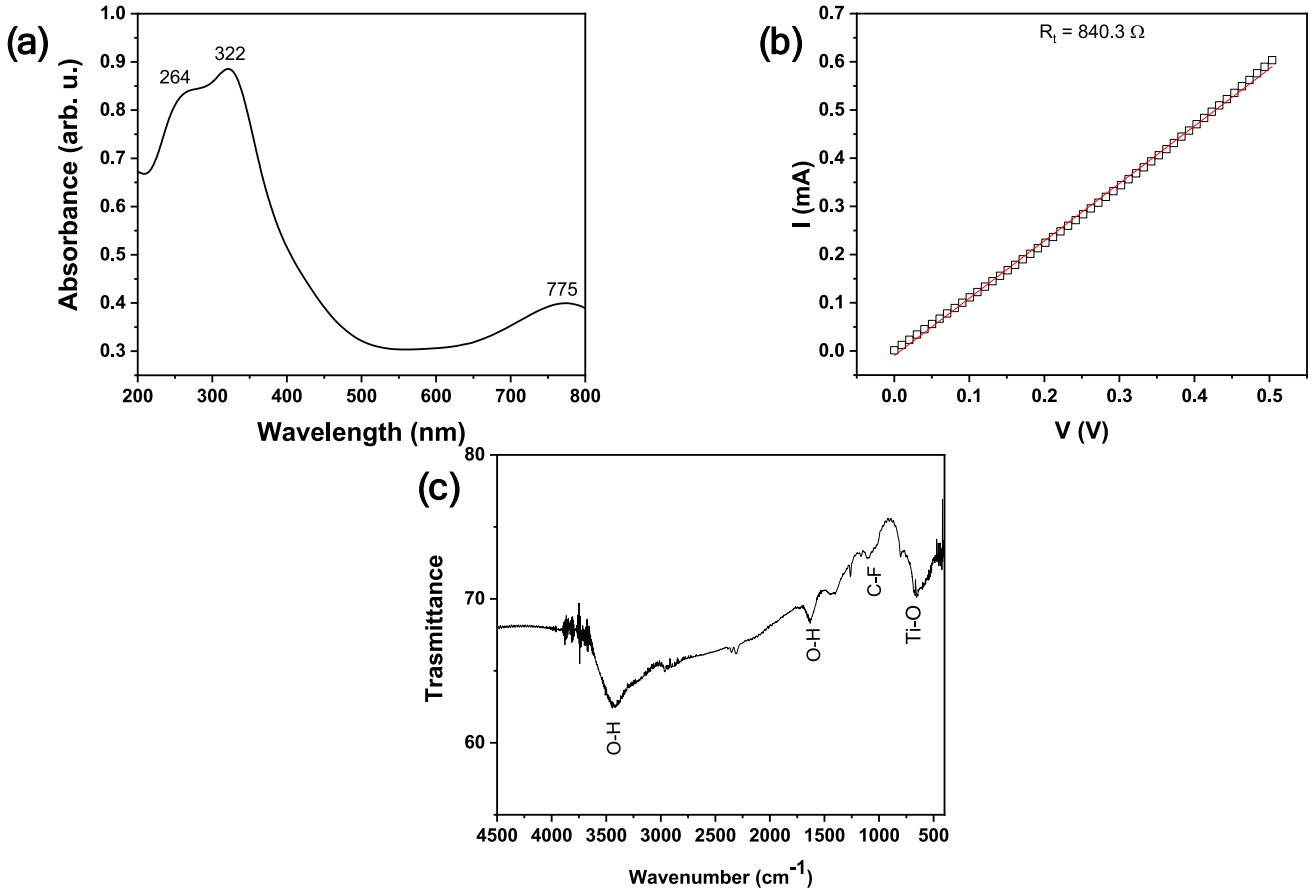

Fig. 3 **a** UV–vis spectrum of $Ti_3C_2T_x$ MXene in aqueous dispersion, **b** current–voltage curve of $Ti_3C_2T_x$ MXene impregnated in cotton textile, and **c** FTIR spectrum of $Ti_3C_2T_x$ MXene powder

respectively, acquired at contact forces of 0.5 N, 1.5 N, and 2.0 N, respectively. Corresponding short-circuit current values are shown for the device at imposed contact forces of 0.5 N (Fig. 4d), 1.5 N (Fig. 4e), and 2.0 N (Fig. 4f).

As observed in the curves for current and voltage of TENGs under different applied forces and operating frequencies, higher positive values than negative ones are typically obtained. Such behavior has been attributed to the sticking effect [37], which describes the asymmetry in the vertical contact/separation process and results in distinct charge transfer during the ascending/descending forces stages.

Another critical aspect of the results is the direct dependence of voltage and current on frequency and force. The literature also reports that increased charge transfer is associated with a higher operating frequency [15, 38] and a higher rate of charge accumulation at interfaces. In addition, the current (see Eq. S11) varies directly with the velocity ($v(t)$), which is proportional to the operating frequency. In terms of force, the positive relationship between electrical output and increasing force results from the greater deformation of tribolayers at higher force, which optimizes charge transfer between the parts.

In addition to measuring the device's electrical response under open-circuit and short-circuit conditions, determining the current and voltage at varying load resistances is a critical characterization for evaluating TENG performance. The results presented in Fig. 5a confirm the general behavior: a decrease in output current with increasing load resistance. At the same time, the voltage increases with increasing load resistance (reducing the transferred charge and increasing the induced charges on the electrode). The opposite variation profile of current and voltage results in a normal distribution of power density, with a maximum at 42.29 μW/cm^2 at an intermediate load resistance (due to the crossover of the current and voltage curves *vs.* load resistance), characterizing the

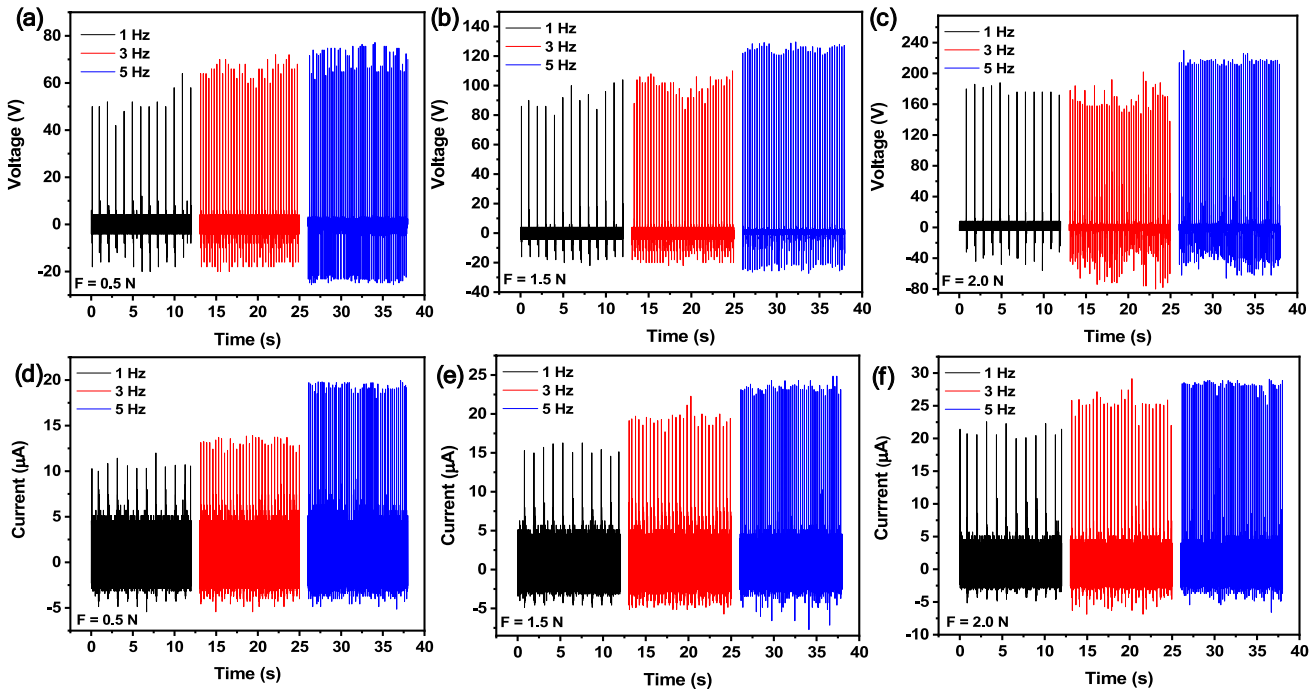

Fig. 4 Open circuit voltage for $Ti_3C_2T_x$ MXene-modified textile electrode acquired at contacting force of 0.5 N (**a**), 1.5 N (**b**), and 2 N (**c**) and short circuit current acquired at contacting force of 0.5 N (**d**), 1.5 N (**e**), and 2 N (**f**). For all curves, the color scheme indicates the operating frequency: black curves were acquired at 1 Hz, red at 3 Hz, and blue at 5 Hz

best experimental condition for the device's operation (Fig. 5b).

The TENG's transferred charge capability was evaluated by connecting it to a full-bridge rectifier and conventional capacitors of 1 μF, 4.7 μF, and 10 μF. As shown in Fig. 5c, a higher value of slope in the voltage–time curve is observed for capacitors with lower capacitance, due to a fixed amount of transferred charge and the inverse relationship with capacitance $\left(V = \frac{Q}{C}\right)$ i.e., higher capacitance with the same charge transfer rate results in a lower voltage at the capacitor terminals. Another critical aspect to consider is the retention of device performance, measured by the open-circuit voltage during repeated cycles of vertical contact-separation. As shown in Fig. 5d, negligible degradation in the response of the TENG is obtained at continuous TENG operation (3,000 cycles of operation).

The operating principle of the device's energy generation mechanism is summarized in the cyclic process depicted in Figs. 6a-d. Considering the tribopositive skin and the tribonegative Ecoflex layer as a pair, the first step of electrification is obtained under contact between the parts, and the voltage is zero (see first image in Fig. 6e). Then, under the releasing force of charged surfaces, the potential difference increases, inducing the accumulation of opposite charges on the electrode. This process continues until the finger reaches its maximum distance from the Ecoflex layer, corresponding to the maximum distance of the finger and the Ecoflex layer (see the sequence of increasing distances in Fig. 6e—from left to right). In the reverse motion, pressing the layers again, there is a reduction in the voltage and the charge flux in the reverse direction is established, reaching the short circuit condition (V = 0 V) when full contact is achieved.

A comparison with corresponding devices that explore the skin as a tribopositive layer or MXene in the composition of overall TENGs is summarized in Table 1, where device performance is detailed in terms of open-circuit voltage, short-circuit current, and power output. As can be seen, the performance of the reported TENG is competitive in comparison with the devices by the direct comparison of the voltage, current and power density, characterizing this device as a promising template for several applications.

Standard applications for the resulting device include powering small electronics (e.g., LEDs) and

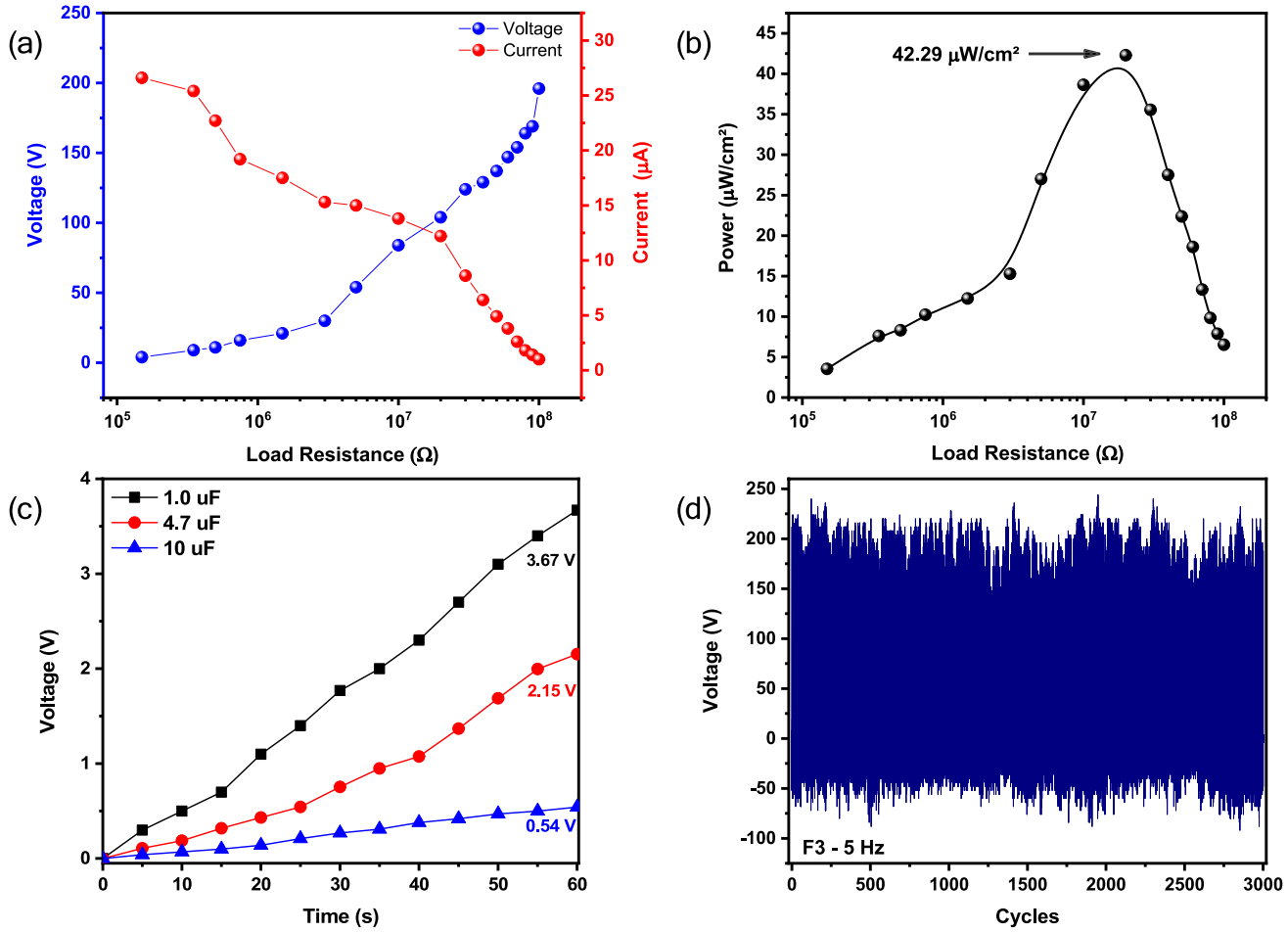

Fig. 5 **a** Voltage and current output of the TENG device at varying load resistance, **b** power density as a function of the load resistance, **c** voltage between terminals of the conventional capacitors as a function of time of operation, and **d** open circuit voltage of the TENG generated by continuous operation process (3,000*x*)

serving as a prototype for tactile sensors. As a proof-of-concept, a circuit was developed (schematically illustrated in Fig. 7) to recognize a two-level response (yes/no) from the simple contact of a finger and the assembled TENG.

As shown, two TENGs were placed side by side, with their output voltages rectified by independent full-bridge rectifiers and connected in parallel to the analog input of a microcontroller (channel A_0 for YES and channel A_1 for NO). The identification of a peak in a specific channel activates a particular message in the speaker (YES or NO in the present application). Video S1 summarizes the overall process of using the implemented circuit. This prototype is of interest for its potential to improve communication with patients in a hospital, enabling communication through a simple touch of a modified textile (which can be incorporated into the patient's clothes). In addition, to illustrate the device's operation by lighting an LED, a video (see video S2) is provided showing the TENG output connected to a full-bridge rectifier in parallel with a 1 μF capacitor, with a switch between the rectifier's terminals and an LED. After a few TENG operations, the energy is stored in the capacitor and then transferred to the LED when the switch is pressed.

4 Conclusion

The impregnation of $Ti_3C_2T_x$ MXene into cotton textiles is achieved through a straightforward approach to impart electrical conductivity to intrinsically insulating cotton fibers. The resulting conductive fabric was used in a single-electrode TENG configuration, in

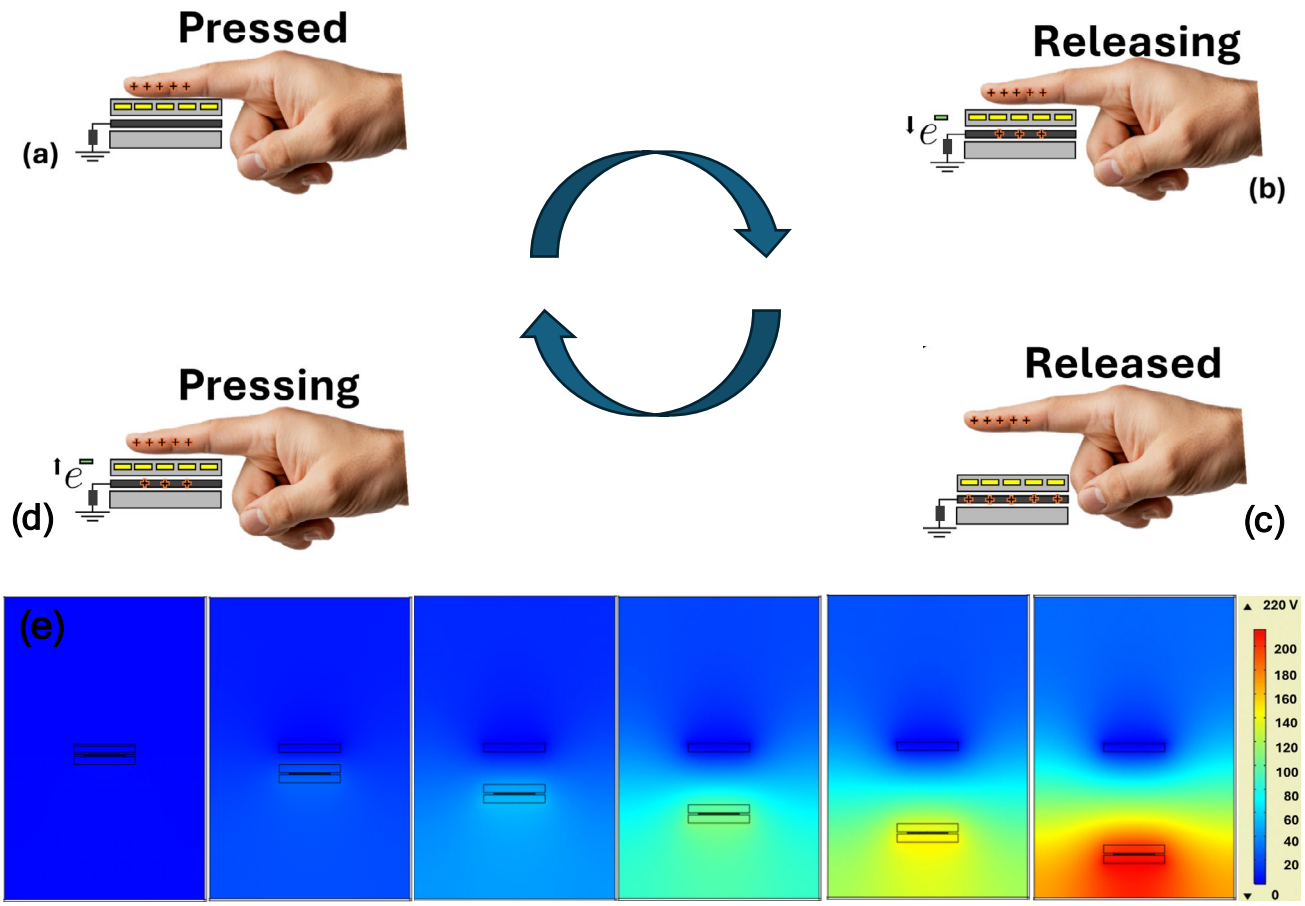

Fig. 6 General mechanism of TENG operation in a complete cycle of vertical contact separation process: **a** contact between parts under pressure, **b** releasing of parts with increasing distance **c** final step of release (maximum distance between the layers), **d** pressing step with the reduction of distance between pairs, and **e** simulated output voltage with the progressive separation of tribopairs carried out considering the experimental limiting voltage values and theoretical values for constants of materials summarized in Table S1

Table 1 Comparison of electrical performance of the reported TENG and corresponding experimental systems reported in the literature (PVA: Polyvinyl alcohol; PEDOT: PSS—poly (3, 4-ethylenedioxythiophene) polystyrene sulfonate; PTFE: Polytetrafluoroethylene; PDMS: Polydimethylsiloxane; WPU: Polyurethane; CNF: Cellulose nanofiber)

Electrode layer	Tribopositive pair	Tribonegative pair	V_{oc} (V)	I_{sc} (μA)	Power density (mW/m^2)	Ref
MXene/PVA hydrogel	Kapton	Silicone rubber	230.0	0.2	330	[39]
MXene/PEDOT:PSS film	MXene/PEDOT:PSS film	PTFE	17.0	0.3	–	[40]
Al foil	Nylon	MXene/PDMS	45.0	0.6	–	[41]
MXene / AgNWs / MXene / Polyurethane	Skin	PDMS	38.0	0.4	7.22	[42]
AgMPs / MXene	WPU	Silicone rubber	114.7	0.8	186.8	[43]
MXene / CNF	Skin	Silicone rubber	400.0	0.7	40.0	[20]
MXene fabric	Skin	Silicone rubber	220.5	28.3	422.9	This work

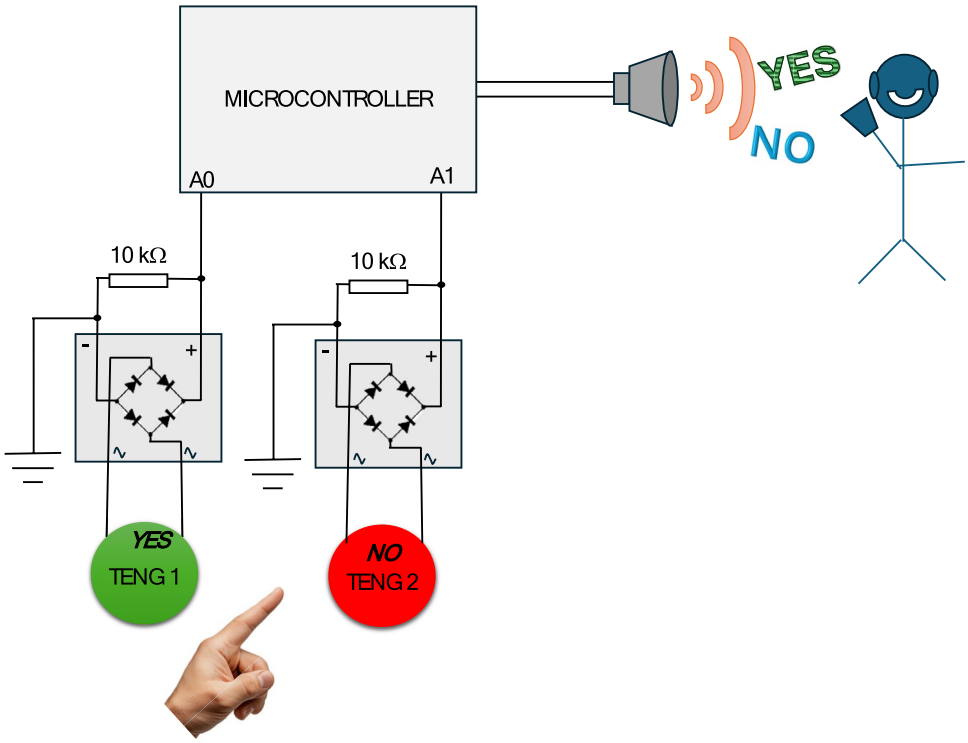

Fig. 7 General scheme of a circuit composed of two TENGs integrated into a two-level system, with the output connected to a microcontroller that identifies the response and provides sound feedback through a speaker

which the finger contact with the Ecoflex-encapsulated electrode generates an open-circuit voltage of 220 V. This performance enables effective energy harvesting for powering small electronic devices and allows its application as a tactile sensor. Furthermore, a prototype touch sensor integrated into an electronic system is proposed for sound-based communication via simple finger contact with a surface, providing an effective means of patient interaction in hospital environments. The findings underscore the role of $Ti_3C_2T_x$ MXene in enhancing textile-based electrodes and open new avenues for developing multifunctional, skin-compatible energy systems tailored for next-generation wearable electronics.

Acknowledgements

This work was financed in part by the Coordenação de Aperfeiçoamento de Pessoal de Nivel Superior (CAPES) –Finance Code 001, CNPq (303997/2021-4, 173177/2024-7, 409215/2022-8, 309614/2021-0 and 302178/2025-2), FINEP, FAPESP (2024/13749-4, 2024/02239-5, 2021/11965-3, 2017/50334-3) and FACEPE. The authors thank the National Institutes of Science and Technology (INCTs), INCT Polysaccharides (Grant: 406973/2022-9), INCT Circularity Polymer Materials (Grant: 406925/2022-4), and INCT-INFO (National Institute of Photonics).

Authors contribution

I.C.M.C. and H.P.O. wrote the main manuscript text, I.C.M.C. prepared figures. All authors discussed the results and reviewed the manuscript.

Funding

The Article Processing Charge (APC) for the publication of this research was funded by the Coordenação de Aperfeiçoamento de Pessoal de Nível Superior - Brasil (CAPES) (ROR identifier: 00x0ma614). Brazilian Funding Agencies CNPq, FINEP, FACEPE, FAPESP, CAPES, and National Institutes of Science and Technology (INCTs).

Data availability

Data will be made available on reasonable request.

Declarations

Conflict of interest On behalf of all authors, the corresponding author states that there is no conflict of interest

Supplementary Information The online version contains supplementary material available at https://doi.org/10.1007/s10854-026-16790-3.

References

1. Y. Du, Z.L. Wang, D. Wei, Emerging sensing systems based on triboelectric nanogenerator. Nano Energy **143**, 111292 (2025). https://doi.org/10.1016/j.nanoen.2025.111292
2. C. Xu, Y. Song, M. Han, H. Zhang, Portable and wearable self-powered systems based on emerging energy harvesting technology. Microsyst. Nanoeng. **7**, 25 (2021). https://doi.org/10.1038/s41378-021-00248-z
3. J. Hui, H. Mao, Role of portable and wearable sensors in era of electronic healthcare and medical internet of things. Clinical eHealth **4**, 62–66 (2021). https://doi.org/10.1016/j.ceh.2021.11.001
4. T. Ahmed, R. Jose, M.M. Alam, R. Crispin, T. Nuge, V. Raj, M.S.M. Saheed, Stretchable surfaces and electrodes for triboelectric nanogenerators: challenges and opportunities. Nano Energy **142**, 111244 (2025). https://doi.org/10.1016/j.nanoen.2025.111244
5. F.R. Fan, Z.Q. Tian, Z.L. Wang, Flexible triboelectric generator! Nano Energy **1**, 328–334 (2012). https://doi.org/10.1016/j.nanoen.2012.01.004
6. D. Doganay, M.B. Durukan, M. Cugunlular, O. Cakir, M.O. Cicek, O. Demircioglu, D. Wei, H.E. Unalan, Triboelectric nanogenerators from fundamentals to applications. Nano Energy **138**, 110825 (2025). https://doi.org/10.1016/j.nanoen.2025.110825
7. D. Choi, Y. Lee, Z.-H. Lin, S. Cho, M. Kim, C.K. Ao, S. Soh, C. Sohn, C.K. Jeong, J. Lee, M. Lee, S. Lee, J. Ryu, P. Parashar, Y. Cho, J. Ahn, I.-D. Kim, F. Jiang, P.S. Lee, G. Khandelwal, S.-J. Kim, H.S. Kim, H.-C. Song, M. Kim, J. Nah, W. Kim, H.G. Menge, Y.T. Park, W. Xu, J. Hao, H. Park, J.-H. Lee, D.-M. Lee, S.-W. Kim, J.Y. Park, H. Zhang, Y. Zi, R. Guo, J. Cheng, Z. Yang, Y. Xie, S. Lee, J. Chung, I.-K. Oh, J.-S. Kim, T. Cheng, Q. Gao, G. Cheng, G. Gu, M. Shim, J. Jung, C. Yun, C. Zhang, G. Liu, Y. Chen, S. Kim, X. Chen, J. Hu, X. Pu, Z.H. Guo, X. Wang, J. Chen, X. Xiao, X. Xie, M. Jarin, H. Zhang, Y.-C. Lai, T. He, H. Kim, I. Park, J. Ahn, N.D. Huynh, Y. Yang, Z.L. Wang, J.M. Baik, D. Choi, Recent advances in triboelectric nanogenerators: from technological progress to commercial applications. ACS Nano **17**, 11087–11219 (2023). https://doi.org/10.1021/acsnano.2c12458
8. A.L. Freire, L.R. Lima, I.C.M. Candido, L.G. Silva, S.J.L. Ribeiro, E. Carrilho, T.L. Oliveira, L.F.C. de Oliveira, H.S. Barud, H.P. de Oliveira, Metal-free, bio-triboelectric nanogenerator based on a single electrode of bacterial cellulose modified with carbon black. Nanoenergy Advances **4**, 110–121 (2024). https://doi.org/10.3390/nanoenergyadv4010006
9. M.-K. Seo, P. Pandey, J.I. Sohn, Metal-free flexible triboelectric nanogenerator based on bifunctional carbon fiber for mechanical energy harvesting and human activity monitoring. Sensors Actuators A Phys. **370**, 115247 (2024). https://doi.org/10.1016/j.sna.2024.115247
10. A.L. Freire, L.R. Lima, I.C.M. Candido, L.G. Silva, S.J.L. Ribeiro, E. Carrilho, T.L. Oliveira, L. Fernando, C. De Oliveira, H.S. Barud, H.P. De Oliveira, Metal-free, bio-triboelectric nanogenerator based on a single electrode of bacterial cellulose modified with carbon black. Nanoenergy Adv. **4**, 110–121 (2024). https://doi.org/10.3390/NANOENERGYADV4010006
11. I. Aazem, D.T. Mathew, S. Radhakrishnan, K.V. Vijoy, H. John, D.M. Mulvihill, S.C. Pillai, Electrode materials for stretchable triboelectric nanogenerator in wearable

electronics. RSC Adv. **12**, 10545–10572 (2022). https://doi.org/10.1039/D2RA01088G

12. A.L. Freire, I.C.M. Candido, H.P. de Oliveira, Polyaniline-based electrodes for flexible woven triboelectric nanogenerators. Mater. Lett. **360**, 136018 (2024). https://doi.org/10.1016/j.matlet.2024.136018
13. P. Zhao, G. Bhattacharya, S.J. Fishlock, J.G.M. Guy, A. Kumar, C. Tsonos, Z. Yu, S. Raj, J.A. McLaughlin, J. Luo, N. Soin, Replacing the metal electrodes in triboelectric nanogenerators: high-performance laser-induced graphene electrodes. Nano Energy **75**, 104958 (2020). https://doi.org/10.1016/j.nanoen.2020.104958
14. B. Xie, Y. Guo, Y. Chen, H. Zhang, J. Xiao, M. Hou, H. Liu, L. Ma, X. Chen, C. Wong, Advances in graphene-based electrode for triboelectric nanogenerator. Nano-Micro Lett. **17**, 17 (2025). https://doi.org/10.1007/s40820-024-01530-1
15. I.C.M. Candido, GdaS. Oliveira, S.J.L. Ribeiro, M. Cavicchioli, H.S. Barud, L.G. Silva, H.P. de Oliveira, PVA-silk fibroin bio-based triboelectric nanogenerator. Nano Energy **105**, 108035 (2023). https://doi.org/10.1016/j.nanoen.2022.108035
16. I.C.M. Candido, G.D.S. Oliveira, G.G. Viana, F.A.G. Da Silva, M.M. Da Costa, H.P. De Oliveira, Wearable triboelectric nanogenerators based on chemical modification of conventional textiles for application in electrically driven antibacterial devices. ACS Appl. Electron. Mater. **4**, 334–344 (2022). https://doi.org/10.1021/acsaelm.1c01028
17. R. Xia, R. Zhang, Y. Jie, W. Zhao, X. Cao, Z. Wang, Natural cotton-based triboelectric nanogenerator as a self-powered system for efficient use of water and wind energy. Nano Energy **92**, 106685 (2022). https://doi.org/10.1016/j.nanoen.2021.106685
18. B.K. Dejene, A.Y. Melese, Textile-based triboelectric nanogenerators: a critical review of materials, fabric designs, and washability for wearable applications. J. Sci.: Adv. Mater. Devices **10**, 100975 (2025). https://doi.org/10.1016/j.jsamd.2025.100975
19. S. Wang, M. He, A flexible triboelectric nanogenerator-enabled insole for self-powered gait monitoring in football applications. Energy Rep. **14**, 803–812 (2025). https://doi.org/10.1016/j.egyr.2025.06.041
20. J. Fan, M. Yuan, L. Wang, Q. Xia, H. Zheng, A. Zhou, MXene supported by cotton fabric as electrode layer of triboelectric nanogenerators for flexible sensors. Nano Energy **105**, 107973 (2023). https://doi.org/10.1016/j.nanoen.2022.107973
21. K. Aiswarya, M. Navaneeth, L. Bochu, P. Kodali, R.R. Kumar, S.K. Reddy, Wrinkled PDMS/MXene composites: a pathway to high-efficiency triboelectric nanogenerators. Mater. Sci. Semicond. Process. **198**, 109739 (2025). https://doi.org/10.1016/j.mssp.2025.109739
22. Q. Liu, X. Chen, X. Wei, J. Sun, C. Liu, Self-powered wearable triboelectric nanogenerator based on MXene/chitosan/carbon nanotube layered composite film. Chem. Eng. J. **517**, 164570 (2025). https://doi.org/10.1016/j.cej.2025.164570
23. R. Wei, S. Sun, A MXene-based double-network conductive hydrogel triboelectric nanogenerator for intelligent sports monitoring. Energy Rep. **13**, 3773–3781 (2025). https://doi.org/10.1016/j.egyr.2025.03.028
24. S. Zhang, M. Guo, Y. Xia, S. Li, X. Zhi, X. Wang, Non-contact monolayered triboelectric nanogenerator based on stretchable MWCNTs/MXene/Ecoflex film for human–machine interface and high-accuracy handwritten recognition. Chem. Eng. J. **505**, 159562 (2025). https://doi.org/10.1016/j.cej.2025.159562
25. J.A.A. Fotius, M.H.M. Facure, D.S. Correa, E. Carrilho, H. da Silva Barud, H.P. de Oliveira, Ti3C2Tx MXene/alginate-based electrodes for supercapacitors. J. Mater. Res. **40**, 1417–1432 (2025). https://doi.org/10.1557/s43578-025-01588-6
26. S.S.K. Mallineni, H. Behlow, R. Podila, A.M. Rao, A low-cost approach for measuring electrical load currents in triboelectric nanogenerators. Nanotechnol. Rev. **7**, 149–156 (2018). https://doi.org/10.1515/ntrev-2017-0178
27. G. Kumar, A. Ahlawat, H. Bhardwaj, G.K. Sahu, P.S. Rana, P.R. Solanki, Ultrasonication-assisted synthesis of transition metal carbide of MXene: an efficient and promising material for photocatalytic organic dyes degradation of rhodamine B and methylene blue in wastewater. Environ. Sci. Pollut. Res. **31**, 38232–38250 (2024). https://doi.org/10.1007/s11356-024-33505-5
28. M. Rahman, M.S. Al Mamun, T. Takaoka, T. Komeda, M. Aly Saad Aly, M. Nasiruddin, S. Islam, M.F. Rahman, W. Alahmad, Synthesis, characterization and catalytic activity of polyethylene glycol (PEG) functionalized MXene ($Ti_3C_2T_x$). ChemistrySelect (2025). https://doi.org/10.1002/slct.202501044
29. A. VahidMohammadi, J. Rosen, Y. Gogotsi, The world of two-dimensional carbides and nitrides (MXenes). Science (2021). https://doi.org/10.1126/science.abf1581
30. Z. Wu, J. Shen, Z. Li, S. Liu, Y. Zhou, K. Feng, B. Zhang, S. Zhao, D. Xue, J. He, K. Yu, J. Zhang, G. Dawson, Q. Zhang, L. Huang, C. Li, X. An, L. Chi, X. Zhang, L. He, Anisotropic plasmon resonance in Ti 3 C 2 T x MXene enables site-selective plasmonic catalysis. ACS Nano **19**, 1832–1844 (2025). https://doi.org/10.1021/acsnano.4c17316

31. P. Tetiana, Z. Danzhen, B. David, S. Kateryna, D. Marley, V. Geetha, I. Alex, C. Benjamin, Z. Teng, S. Christopher E., H. Yong-Jie, G. Yury, Fourier-transform infrared spectral library of MXenes. Chem. Mater. **36**, 8437–8446 (2024). https://doi.org/10.1021/acs.chemmater.4c01536
32. A. Furchner, T. Parker, V. Mauchamp, S. Hurand, J. Plaickner, J. Rappich, A.A. Emerenciano, K. Hinrichs, Y. Gogotsi, T. Petit, Ti 3 C 2 T x MXene thin films and intercalated species characterized by IR-to-UV broadband ellipsometry. J. Phys. Chem. C **129**, 500–507 (2025). https://doi.org/10.1021/acs.jpcc.4c06906
33. X. Sithole, L.Q. Qwabe, L.N. Dlamini, A double transition metal MXene/S-scheme heterojunction composite with improved photoelectrochemical and photocatalytic properties. Mater. Today Commun. **40**, 110233 (2024). https://doi.org/10.1016/j.mtcomm.2024.110233
34. Z. Liu, H. Lv, Y. Xie, J. Wang, J. Fan, B. Sun, L. Jiang, Y. Zhang, R. Wang, K. Shi, A 2D/2D/2D Ti 3 C 2 T x @TiO 2 @MoS 2 heterostructure as an ultrafast and high-sensitivity NO 2 gas sensor at room-temperature. J. Mater. Chem. A. **10**, 11980–11989 (2022). https://doi.org/10.1039/D1TA09369J
35. Y. Li, X. Zhou, J. Wang, Q. Deng, M. Li, S. Du, Y.-H. Han, J. Lee, Q. Huang, Facile preparation of in situ coated Ti 3 C 2 T x /Ni 0.5 Zn 0.5 Fe 2 O 4 composites and their electromagnetic performance. RSC Adv. **7**, 24698–24708 (2017). https://doi.org/10.1039/C7RA03402D
36. M.H.M. Facure, L.A. Mercante, Y. Gogotsi, D.S. Correa, ZnO–Co 3 O 4 nanofibers/MXene composite with peroxidase-like activity for ascorbic acid detection. ACS Appl. Nano Mater. **8**, 4291–4299 (2025). https://doi.org/10.1021/acsanm.4c00539
37. R.D.I.G. Dharmasena, Inherent asymmetry of the current output in a triboelectric nanogenerator. Nano Energy **76**, 105045 (2020). https://doi.org/10.1016/J.NANOEN.2020.105045
38. I.C.M. Candido, L.F. Piovesan, A.L. Freire, J.A.A. Fotius, J.J.I. de Lima, H.S. Barud, H.P. de Oliveira, Biodegradable hyaluronic acid-based triboelectric nanogenerator as self-powered temperature sensor. Mater. Today Commun. **36**, 106855 (2023). https://doi.org/10.1016/j.mtcomm.2023.106855
39. X. Luo, L. Zhu, Y.C. Wang, J. Li, J. Nie, Z.L. Wang, A flexible multifunctional triboelectric nanogenerator based on MXene/PVA hydrogel. Adv. Funct. Mater. **31**, 2104928 (2021). https://doi.org/10.1002/ADFM.202104928
40. Z. Zhang, Q. Yan, Z. Liu, X. Zhao, Z. Wang, J. Sun, Z.L. Wang, R. Wang, L. Li, Flexible MXene composed triboelectric nanogenerator via facile vacuum-assistant filtration method for self-powered biomechanical sensing. Nano Energy **88**, 106257 (2021). https://doi.org/10.1016/j.nanoen.2021.106257
41. D. Wang, Y. Lin, D. Hu, P. Jiang, X. Huang, Multifunctional 3D-MXene/PDMS nanocomposites for electrical, thermal and triboelectric applications. Compos. Part A Appl. Sci. Manuf. **130**, 105754 (2020). https://doi.org/10.1016/j.compositesa.2019.105754
42. J. Liu, L. Zhang, N. Wang, C. Li, Highly stretchable and transparent triboelectric nanogenerator based on multilayer structured stable electrode for self-powered wearable sensor. Nano Energy **78**, 105385 (2020). https://doi.org/10.1016/j.nanoen.2020.105385
43. Y. Jia, Y. Pan, C. Wang, C. Liu, C. Shen, C. Pan, Z. Guo, X. Liu, Flexible Ag microparticle/MXene-based film for energy harvesting. Nano-Micro Lett. **13**, 201 (2021). https://doi.org/10.1007/s40820-021-00729-w